Pertanika J. Sci. & Technol. 34 (4): 2359 - 2384 (2026)

SCIENCE & TECHNOLOGY

Journal homepage: http://www.pertanika.upm.edu.my/

Impact of Wind Farm Penetration on the Mal-Operation of Distance Relay Power Swing Blocking and Out-of-Step Functions

Chidiebere Okeke[1], Mohammad Lutfi Othman[1]*, Hashim Hizam[1], Mohd Zainal Abdin Ab Kadir[1], Samuel Nwagbara[1], Osaji Emmanuel[1,2], Jude Aneke[3], Okeke Ugochukwu Kingsley[3], and Masoud Ahmadipour[4]

[1]*Advanced Lightning, Power and Energy Research (ALPER), Department of Electrical and Electronic Engineering, Faculty of Engineering, Universiti Putra Malaysia, 43400 UPM Serdang, Selangor, Malaysia.*
[2]*Department of Electrical and Electronic Engineering, Faculty of Engineering, Federal University Lokoja, P.M.B. 1154 Lokoja, Kogi State, Nigeria*
[3]*Department of Electrical Engineering, Faculty of Engineering, Nnamdi Azikiwe University, P.M.B. 5025 Awka, Anambra State, Nigeria*
[4]*School of Electrical Engineering, College of Engineering, Universiti Teknologi MARA, 40450 Shah Alam, Selangor, Malaysia*

ABSTRACT

The increasing penetration of wind energy conversion systems into modern power grids has introduced significant challenges to transmission line protection schemes. Among these, distance relays equipped with power swing blocking and out-of-step tripping functions are particularly affected due to variations in apparent impedance trajectories during transient disturbances. This study investigates the impact of wind farm penetration on the mal-operation of distance relay power swing blocking and out-of-step functions using a modified IEEE 6-Bus Network integrated with a 10 MW Doubly-Fed Induction Generator (DFIG) wind farm. First, the analysis was performed using the conventional Power Swing Blocking (PSB) and Out-of-Step (OST) protection scheme, which were based on deterministic criteria such as blinders, impedance trajectory analysis, and rate of change of impedance measurements. The analysis was expanded by employing a modified intelligent PSB and OST protection scheme based on a hybrid signal processing and machine learning methodology. The paper focuses on analysing the dynamic behaviour of impedance loci, the resulting relay behaviour and performance under changing degrees of DFIG wind farm penetration. Time-domain simulations

ARTICLE INFO

Article history:
Received: 27 March 2026
Accepted: 21 July 2026
Published: 20 August 2026

DOI: https://doi.org/10.47836/pjst.34.4.20

E-mail addresses:
chidiebereokekea@gmail.com (Chidiebere Okeke)
lutfi@upm.edu.my (Mohammad Lutfi Othman)
hhizam@upm.edu.my (Hashim Hizam)
mzk@upm.edu.my (Mohd Zainal Abdin Ab Kadir)
sammytotti@gmail.com (Samuel Nwagbara)
emmanuel.osaji@fulokoja.edu.ng (Emmanuel Osaji)
anekejude@gmail.com (Jude Aneke)
kingsleyokeke2040@gmail.com (Ugochukwu Okeke)
masoud@uitm.edu.my (Masoud Ahmadipour)
* Corresponding author

e-ISSN: 2231-8526

were conducted to evaluate relay performance under stable and unstable swing conditions. The obtained results showed that higher levels of wind penetration affected both the magnitude of fault current contribution and the dynamic behaviour of the system, which resulted in changes to the apparent impedance trajectory seen by the distance relay. These changes influenced the operation of the PSB and OST, which led to delayed blocking actions or unwanted relay trips in some scenarios. This study highlighted the importance of protection coordination when integrating large amounts of wind generation into transmission networks.

Keywords: DFIG, distance relay, out-of-step tripping protection, power swing blocking, renewable energy integration, wind penetration.

INTRODUCTION

To ensure operational reliability and mitigate equipment failure or damage during grid disturbances, modern electrical power systems depend heavily on protective relays. Fast response and selective tripping capabilities have been one of the major criteria for choosing protective devices, and distance relays among various protection devices are heavily used for the protection of high-voltage transmission lines for this reason. The apparent impedance between the fault points and the relay location is very crucial for the protective relays, as they perform their function by measuring and using this impedance (Fischer et al., 2012; Mooney & Fischer, 2006). The estimated apparent impedance stays outside the relay tripping zones under no-fault conditions, but once a disturbance occurs, such as faults or power swings, the relay operation is triggered because a part of this apparent impedance will fall into the protection zones (Zhang et al., 2016).

In synchronous generators, a temporary imbalance between electrical output power and mechanical input power gives rise to power swing disturbances. Line switching, faults, sudden load changes, or generator outages usually contribute to such disturbances (Audu et al., 2018; Wei et al., 2014). In the event of a power swing, the oscillation of the rotor angle of synchronous generators leads to voltage and current fluctuations (Chaitanya et al., 2019). The apparent impedance seen by the distance relays is heavily affected by the oscillations, which leads to unwanted tripping of the relay (Abdi-Khorsand & Vittal, 2016).

From a technical point of view, there are broadly two kinds of power swings: unstable and stable power swings. When a system returns to a new steady-state operating point after a perturbation, it is referred to as a stable power swing, but when a perturbation causes the generators to lose synchronism and continue to accelerate until it results in system failure, it is referred to as an unstable swing (Paudyal et al., 2010; Nasab & Yaghobi, 2020).

For protection reliability, additional functions referred to as Power Swing Blocking (PSB) and Out-of-Step Tripping (OST) are included in the distance relays. The tripping of the distance relay during stable swings is blocked by the Power Swing Blocking function, while the unstable part of the system or grid is isolated in the event of loss of synchronism (Fischer et al., 2012; Gonzalez-Longatt et al., 2021).

However, the conventional distance relay scheme is still subject to huge difficulties in recent power systems, even with this protection mechanism, and this is attributed to the high penetration of renewable energy sources. Like other renewable energy sources, solar photovoltaic (PV) and wind farm systems have dynamic and converter-based characteristics which affect the impedance characteristics of the power system as well as the power system inertia and fault current magnitude (Adak, 2024; Dreidy et al., 2017; Telukunta et al., 2017). These impacts significantly contribute to relay operation and jeopardise the discrimination between fault conditions and actual power swings (Fang et al., 2018; Haddadi et al., 2019).

Given the environmental issues and global migration to sustainable energy solutions, wind energy has been greatly introduced into the power system in the last twenty years at an increasing rate (Kumar et al., 2016; Shair et al., 2021). Due to the capability of doubly fed induction generators (DFIG) to function at variable speeds and provide efficient energy conversion, they are being utilised heavily in wind turbines. Unfortunately, compared with conventional synchronous generators, power electronic converters are being used in DFIG-based wind farms, which alter fault current characteristics (Gautam et al., 2009; Okeke et al., 2023).

The effects of renewable energy infiltration in power system protection have been studied in many research works. Studies have revealed that short-circuit current levels are reduced, and system impedance profiles are manipulated by converter-based generation, which results in relay maloperation (Haddadi et al., 2021; Niknezhad & Sadeh, 2022). Also, relay settings are being impacted negatively by the dynamic operating conditions that come with the wind generation variability (Nwaigwe et al., 2019).

In the past, rate-of-change measurements, impedance-based methods and signal processing techniques, such as power swing detection techniques, have been the focus of research. The rate of change of impedance trajectory has always been the main reliance of the conventional PSB algorithms to differentiate between power swings and faults (Jafari et al., 2014; Kang & Gokaraju, 2016). The challenge is that when the impedance trajectories overlap because of renewable energy infeed currents, these methods can fail (Arumuga & Reddy, 2022).

Intelligent protection methods have been studied in more recent papers, whereby machine learning algorithms and artificial intelligence are employed extensively. This has allowed for the classification of system perturbations based on pattern recognition techniques using voltage and current signals (Chothani et al., 2014). Even though intelligent protection methods are proven to be interesting, the basic impact of renewable energy grid infiltration on relay characteristics should be clearly established (Yellajosula et al., 2019).

Specifically, the apparent impedance seen by the relays can be greatly impacted by the current injected by the wind farm. The current injection by the wind farms if installed very close to the location of the distance relay can change the impedance direction towards the protection zones of the relay and this usually led to unintended tripping of the relay during the occurrence of stable swings or cause delay in tripping of the relay during unstable swings (Haddadi et al., 2019; Niknezhad & Sadeh, 2022; Verzosa 2013).

Hence, it is very important to have good knowledge of the impact of the infiltration of renewable energy current on the protection schemes of relays, especially in ensuring system reliability (Fang et al., 2018; Telukunta et al., 2017).

Unlike previous studies that basically investigated traditional PSB and OST protection techniques based on deterministic criteria such as blinders, impedance trajectory analysis, and rate of change of impedance measurement, this paper improved on that by analysing the impact of increasing DFIG wind farm penetration on the performance of intelligent Distance Relay PSB and OST functions. This was done by developing and validating an intelligent hybrid signal processing machine learning framework for PSB and OST functions under changing renewable penetration levels.

Therefore, studying and understanding the impact of wind farm current injections on the way PSB and OST operate or function in a transmission system is the primary focus of this paper. So, the primary task of this paper is to examine the impact of wind farm current infeed on the ill-operation of distance relay protection schemes. The test object used is the modified IEEE 6-bus system incorporated with a 10MW doubly fed induction wind farm, and robust simulations of fault conditions and power swings have been used to examine how the impedance characteristics and protection performance of the distance relay are impacted by the renewable energy infeed.

MATERIALS AND METHODS

The Modified IEEE 6-Bus Network with Integrated 10 MW DFIG Wind Farm (NT-2)

The chosen system configuration is an IEEE 6-bus grid system with a 9 MW Doubly-Fed Induction Generator (DFIG) wind farm (NT-2), and the study was done using this network. The DFIG dynamic model consists of the standard rotor-side and grid-side converter control loops together with the crowbar protection mechanism available in the MATLAB/Simulink environment. The controller parameters were made to remain constant throughout all wind penetration cases to ensure a consistent comparison of the relay performance.

Figure 1 depicts the system configuration, which is a meshed transmission network having aggregated loads, interconnected transmission lines, and synchronous generators. The wind generation unit is connected to an intermediate bus.

A fraction of the traditional generation capacity was replaced by the wind farm, which allowed the variation of the wind penetration levels to be controlled while ensuring the

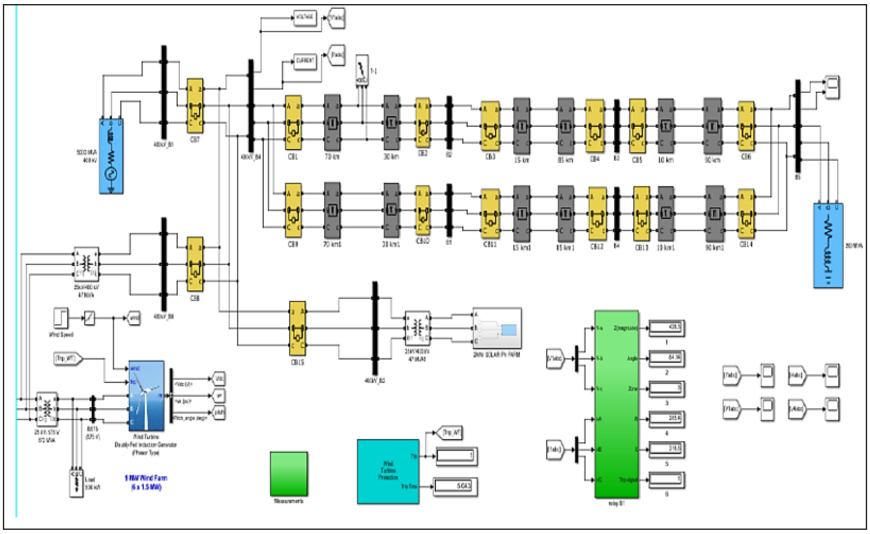

Figure 1. Modified IEEE 6-bus network having a 9 MW DFIG wind farm (NT-2) at an intermediate bus developed in the MATLAB/Simulink environment

total system loading conditions. Using a step-up transformer, the DFIG wind plant, which is rated 9 MW, is linked to the transmission system.

Equation 1 (Khan et al., 2020; Sabo et al., 2020) defines the wind penetration level.

$$WP = \frac{P_w}{P_t} \times 100\% \quad [1]$$

Where:
P_w is the wind farm's active power output, and
P_t is the power system's total generation.

Out-of-Step Tripping (OST) Unit

Differentiating between unstable and stable power swing conditions is very important in distance relay operation because it enhances system reliability, and OST is used to achieve this. The network ultimately restores its stability and assumes a new operating point after going through a small rotor angle displacement during a stable power swing. On the other hand, the system generator loses synchronism, stability, or experiences large-scale power outages during unstable power swings, which is an unwanted operating condition.

To verify the OST operation, a MATLAB/Simulink model was implemented to simulate the response of the relay during various power swing conditions. The model provides a benchmark for the minimum acceptable discrepancy between the monitored current and voltage signals. This benchmark mitigates the loss of synchronism of the generator, which is initiated by the huge frequency deviations during out-of-step situations.

MATLAB/Simulink was used to simulate this dynamic behaviour of the power network during these conditions to be able to examine the response of the relay and the OST protection operation performance.

Power Swing Blocking (PSB) Unit

The grouping of the stable swing, unstable swing conditions, and short-circuit faults during both transient and steady-state system conditions is made possible by the modelling of the PSB in the MATLAB/Simulink environment. By differentiating between short-circuit faults and stable power swing conditions, the PSB operation mitigates unwanted tripping of the relay under power swings. The detection mechanism of PSB employs the rate of change of the measured apparent impedance by the distance relay, and to measure the trajectory of the impedance during power swing conditions, a blinder-based blocking method is utilised.

The impedance sensing unit of the relay is integrated with this blocking logic so that during a short-circuit fault scenario, the relay gives a command to trip and isolate the faulted area so as to protect the equipment. On the other hand, the PSB unit prevents the trip command from causing unwanted operation of the relay.

To evaluate the duration of the perturbation, a MATLAB function block was developed, which is constrained to a maximum of 30 cycles. The impedance trajectory under fault conditions and power swing was modelled and simulated, which permits the historical datasets for development of the model to be obtained.

The tripping areas and the blocking for the relay is decided by the blinder block, and the grouping of the scenarios is defined by the rate of change of the impedance as estimated. A swing scenario is determined by how slow the trajectory movement of the impedance is, and, on the contrary, short-circuit faults are determined by fast variation in the impedance. The required response from the relay is defined by the decision logic block, and when the trajectory of the impedance goes into the region of the blinder under a swing, the tripping of the relay is blocked. However, when the trajectory of the impedance goes beyond the region of the blinder during fault conditions, a command to trip is released.

Integrated 9 MW Wind Turbine Modelling

As mentioned earlier, to understand the impact of wind power integration on the false-trip function of distance relays, especially under short-circuit fault conditions and power swing, a renewable energy infiltration was included in this investigation. In MATLAB/Simulink, a model of a 9 MW wind farm was implemented employing 6 units of doubly fed induction generator (DFIG) wind turbines of 1.5 MW each, which depicts a Type-C wind turbine set-up.

Mechanical Power of the Wind Turbine

The mechanical power produced by each 1.5 MW wind turbine unit was estimated using the fundamental wind turbine power equation (Ali et al., 2016; Veerasamy et al., 2021) implemented in MATLAB/Simulink as shown in Equation 2:

$$P = \frac{1}{2}\rho A_T V_w^3 C_p(\lambda, \beta) \qquad [2]$$

Where:
ρ represents the air density ($1.225\ kg/m^3$),
A_T is the turbine swept area (πr^2),
r is the radius of the turbine blade,
V_w^3 is the cube root of the wind speed (average value of 12m/s),
C_p represents the turbine power coefficient (efficiency of the machine),
λ is the tip speed ratio of the turbine, and
β is the blade pitch angle (assumed constant at 0^0).

The MATLAB/Simulink implementation of the mechanical power model (equation) is illustrated in Figure 2.

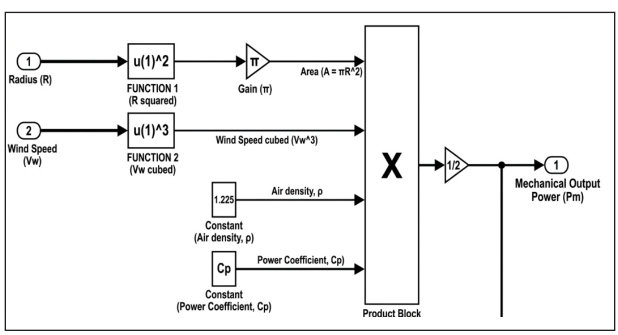

Figure 2. Wind turbine mechanical power model

Intermittent Tip-Speed Ratio Model of the Wind Turbine

The instantaneous tip-speed ratio plays an important role in calculating the turbine power coefficient. The mathematical model used for estimating the intermittent tip-speed ratio is given by Equation 3:

$$\frac{1}{\lambda_i} = \frac{1}{\lambda_T + 0.08\beta} - \frac{0.035}{\beta^3 + 1} \qquad [3]$$

Where the λ_i is the intermittent tip speed ratio of the turbine. The MATLAB/Simulink implementation of this model is shown in Figure 3.

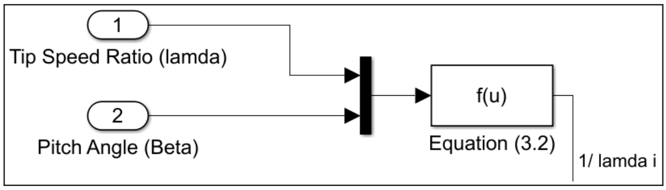

Figure 3. Intermittent tip speed ratio model of the wind turbine

Turbine Power Coefficient Model (Cp)

The turbine power coefficient C_p was modelled using two input parameters: the tip-speed ratio λ and the blade pitch angle β. The relationship is expressed as Equation 4:

$$C_p(\lambda, \beta) = C_1 * \left(\frac{C_2}{\lambda_w} - C_3\beta - C_4\beta^2 - C_5\right) * e^{\frac{-C_6}{\lambda_i}} \quad [4]$$

where C_1–C_6

The turbine design parameters are provided by the manufacturer and summarised in Table 1. The MATLAB/Simulink implementation of this subsystem is illustrated in Figure 4.

Table 1
Wind turbine modelling parameters

Symbol	Values	Parameters Description	Rating
C1	0.5	Rated Power	1.5 MW
C2	116	Rated Wind speed (V_W)	12 m/s
C3	0.4	Pitch angle (β)	0
C4	0	Optimal TSR (λ_T)	8.1
C5	5	Air Density (ρ)	1.225 kg/m³
C6	21	Wind Turbine blade length (r)	33.156 m
Optimal Tip Speed Ratio			2.932 m/s

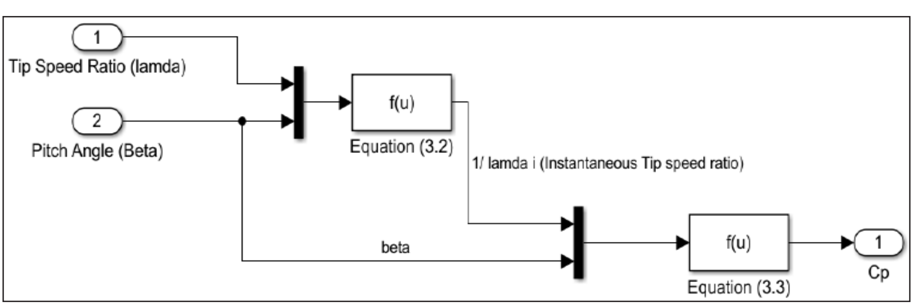

Figure 4. Wind turbine power coefficient model

Optimal Tip Speed Ratio Model of the Wind Turbine

The optimal rotational speed of the wind turbine was determined using the following Equation 5:

$$\lambda_T = \lambda_T^{op} = \frac{W_T + r_T}{V_w} \quad [5]$$

where ω_T represents the turbine rotational speed, r_T is the turbine blade radius, and V_w is the wind speed.

As seen in Figure 5, saturation blocks were incorporated in the Simulink implementation to ensure that the wind speed and tip-speed ratio parameters do not assume zero values, which could cause simulation instability. The lower limits were set to values close to zero, while the upper limits were set to infinity to avoid simulation errors.

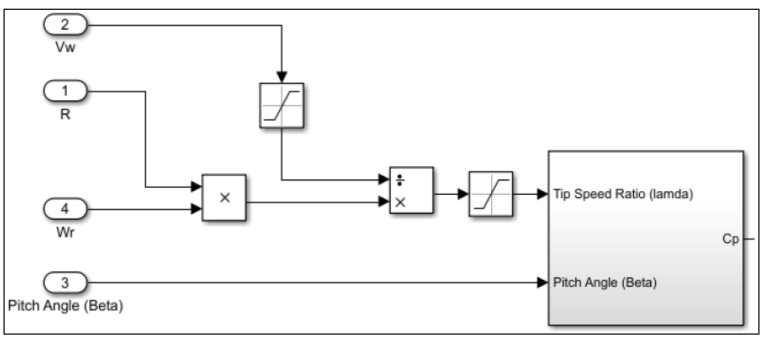

Figure 5. Optimal tip-speed ratio model of the wind turbine

Wind Turbine System Integration

All subsystem models were integrated in MATLAB/Simulink to create the complete 1.5 MW wind turbine model. The model includes four input parameters and two output parameters, as illustrated in Figure 6(a), while the detailed subsystem interconnections are shown in Figure 6(b).

The mechanical power and torque outputs generated by each turbine under transient and steady-state conditions were recorded for further analysis. Six turbine subsystems were connected in parallel to achieve the required 9 MW wind power output before interfacing with the converter system and integrating with the benchmark test network.

Research Workflow

Figure 7 illustrates the overall research workflow adopted in this study. The workflow summarises the modelling process, dataset generation, and development of intelligent machine learning-based PSB and OST protection functions for distance relay systems.

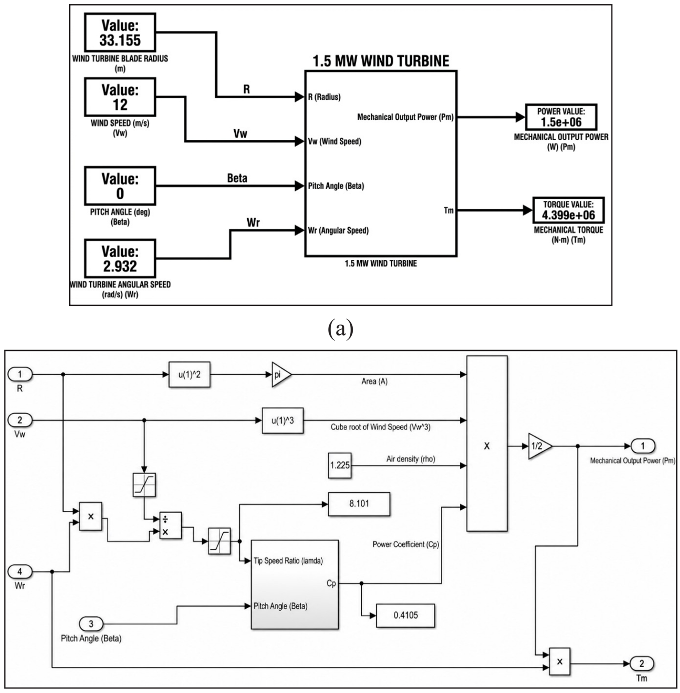

Figure 6. 1.5 MW Wind turbine model: (a) Subsystem block diagram; (b) Internal model architecture

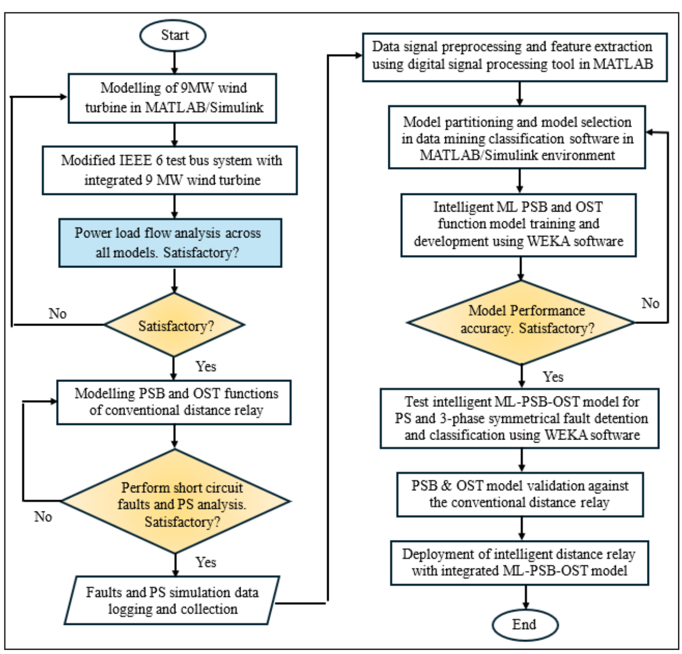

Figure 7. The research workflow

The proposed methodology enables accurate discrimination between power swing events and symmetrical short-circuit faults in renewable energy-integrated power systems.

RESULTS AND DISCUSSION

Power Load Flow Results from Test Bus Benchmark Model

The conducted power load flow analysis across the network presented the voltage magnitudes and phase angles at each bus. The swing bus (Bus 1), to which the 5,000 MVA generator is connected, maintained a voltage magnitude of 1 p.u (400 kV) and supplied the required reactive power (Q), as illustrated in Figure 8. The steady-state load flow analysis performed determined the power delivery capacity of each network component while ensuring compliance with stipulated operational standards. In addition, the direction of active (P) and reactive (Q) power flow across the branch elements is indicated in the load flow results.

The voltage magnitudes and phase angles obtained under steady-state conditions indicate stable and healthy network performance at each bus, supporting the integration of both renewable and non-renewable power sources. Furthermore, the active and reactive

	Block type	Bus type	Bus ID	Vbase (kV)	Vref (pu)	Vangle (deg)	P (MW)	Q (Mvar)	Qmin (Mvar)	Qmax (Mvar)	V_LF (pu)	Vangle_LF (deg)	P_LF (MW)	Q_LF (Mvar)	Block Name	Column2
1	Vsrc	swing	BUS_1	400	1	0	0	0	-Inf	Inf	1	0	1280000	0	5000 MVA 400 kV	
2	Bus	-	BUS_B4	400	1	0	0	0	0	0	0,2	0	0	0	Load Flow Bus1	
3	Bus	-	BUS_2	400	1	0	0	0	0	0	3,815	10,02	0	0	Load Flow Bus2	
4	Bus	-	BUS_5	400	1	0	0	0	0	0	3,814	8,02	0	0	Load Flow Bus3	
5	RLC load 2	-	BUS_3	400	1	0	210	150	0	0	3,014	7,49	0	0	260 MVA	
6	Bus	-	BUS_1	400	1	0	0	0	-Inf	Inf	3,815	11,53	0	0	Load Flow Bus5	
7	Bus	-	BUS_4	400	1	0	0	0	0	0	3,814	9,27	0	0	Load Flow Bus6	
8	Vprog	swing	"1"	120	1	0	0	0	-Inf	Inf	1	0	2,05	11,97	120 kV	
9	Bus	-	"2"	25	1	0	0	0	0	0	0,793	-29,01	0	0	25 kV // 575 V 6*2 MVA	
10	Vsrc	swing	"3"	400	1	0	0	0	-Inf	Inf	1	-127,7	5	293,45	2MW SOLAR PV FARM/10000 MVA 40...	
11	Bus	-	"4"	400	1	0	0	0	0	0	6,519	10,02	0	0	30 km	
12	Bus	-	"5"	400	1	0	0	0	0	0	8,399	9,71	0	0	15 km	
13	Bus	-	"6"	100	1	0	0	0	0	0	8,427	11,19	0	0	15 km	
14	Bus	-	"7"	100	1	0	0	0	0	0	8,427	7,97	0	0	10 km	
15	Bus	-	"8"	100	1	0	0	0	0	0	0,426	9,1	0	0	10 km	
16	Bus	-	"9"	120	1	0	0	0	0	0	0,9951	-0,02	0	0	120 kV // 25 kV 47 MVA	
17	Bus	-	"10"	25	1	0	0	0	0	0	0,7996	-28,93	0	0	Plant 2 MVA // 25 // 2.3 kV 2.6 MVA	
18	Bus	-	"11"	100	1	0	0	0	0	0	3,089	11,53	0	0	70 km	
19	Bus	-	"12"	100	1	0	0	0	0	0	8,362	11,53	0	0	30 km	
20	Bus	-	"13"	100	1	0	0	0	0	0	8,385	11,53	0	0	15 km	
21	Bus	-	"14"	100	1	0	0	0	0	0	8,428	9,27	0	0	85 km	
22	Bus	-	"15"	100	1	0	0	0	0	0	8,357	9,27	0	0	10 km	
23	Bus	-	"16"	100	1	0	0	0	0	0	8,428	7,49	0	0	90 km	
24	Bus	-	"17"	25	1	0	0	0	0	0	1,176	0,02	0	0	25 kV // 400 kV 47 MVA	
25	Bus	-	"18"	100	1	0	0	0	0	0	0,362	10,02	0	0	30 km	
26	Bus	-	"19"	100	1	0	0	0	0	0	8,385	10,02	0	0	15 km	
27	Bus	-	"20"	100	1	0	0	0	0	0	8,428	8,02	0	0	85 km	
28	Bus	-	"21"	100	1	0	0	0	0	0	8,428	8,02	0	0	10 km	
29	Bus	-	"22"	100	1	0	0	0	0	0	8,357	7,49	0	0	90 km	
30	Bus	-	"23"	25	1	0	0	0	0	0	5,878	0,03	0	0	25 kV // 400 kV 47 MVA	
31	Bus	-	"24"	100	1	0	0	0	0	0	4,089	0	0	0	70 km	

Figure 8. Steady-state power load flow results

power flows through the branch elements, including the transmission lines, demonstrate satisfactory operational performance consistent with the requirements of the grid code.

Wind Turbine Penetration Results

The short-circuit fault current penetration at different locations along the transmission line shows a slight increase in magnitude when the wind farm is integrated into the network compared to the scenario without renewable wind energy integration, as illustrated in Figure 9. This slight increase is sufficient to affect the preset impedance estimation used for the trip operation of the distance relay under power swing (PS) and symmetrical three-phase short-circuit fault conditions. The highest level of fault current penetration is observed at fault locations closest to the point of common coupling (PCC), specifically at bus-bar location 4.

The results presented in Table 2 show the current infeed penetration values recorded at the distance relay location, which corresponds to the Point of Common Coupling (PCC), from each interconnected source under different operating conditions. Under normal operating conditions, the synchronous generator (SG) provides the

Table 2
Current infeed estimations at the relay location

Operating Conditions	Current infeed penetrations SG and WF sources		
	SG	**WF**	**Z∠θ**
Normal	810	3.014	429.7-345.5i
Fault Distance (km)	**SG**	**WF**	**Z∠θ**
20	794.9	3.253	258.8-298.3i
40	55.33	3.014	251.6-294i
60	810.8	3.014	249.7-345i
80	810.8	3.014	249-345.51
100	-	-	-

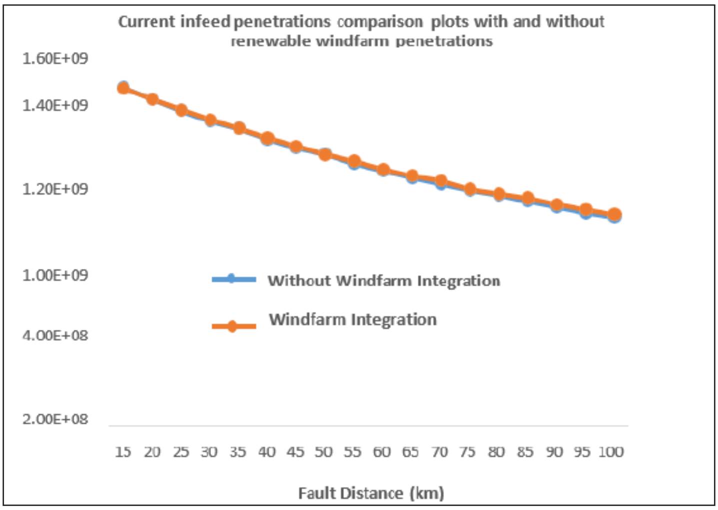

Figure 9. Comparison of current infeed penetration

largest current infeed contribution, while the wind farm contributes only a small fraction of the total current penetration used for impedance estimation by the distance relay, as illustrated in Figure 10.

Although the contribution from the renewable sources is relatively small, it plays a significant role in the mal-operation of the distance relay's Power Swing Blocking (PSB) and Out-of-Step Tripping (OST) functions.

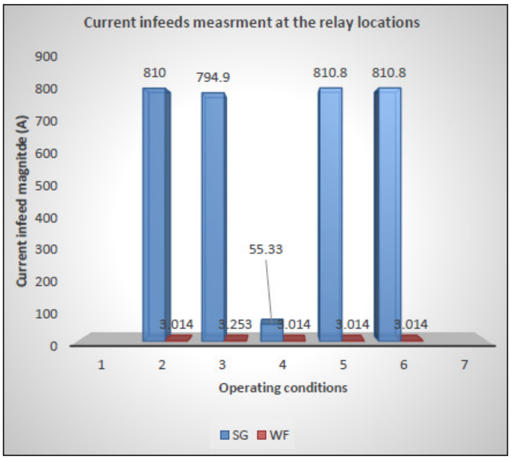

Figure 10. Distance relay infeed current measurement

Conventional Distance Relay Model Performance

The recorded dataset obtained from the conventional distance relay model implemented in MATLAB/Simulink at the Bus 4 terminal demonstrates the estimated line impedances under stable power swing (PS) and short-circuit fault conditions across the four network architectures. This section presents the observed impact of current infeed on the mal operation of the conventional distance relay during power swings and symmetrical short-circuit faults.

The measured power system parameters were used to estimate the impedance locus to support the distance relay's trip decision. The knowledge derived from transient fault voltage and current signals was further utilised to develop the modified intelligent PSB and OST functions.

Fluctuations in the magnitude of current infeed contributions from the integrated renewable energy sources present a significant challenge to the preset trip characteristics of the distance relay, as illustrated in the previously presented results.

Estimated Impedance Under Short-Circuit Faults

The estimated impedance observed by the conventional relay during short-circuit fault conditions at different fault locations is presented in Table 3. These values represent the phasor measurement parameters detected by the distance relay on transmission line L2. The real and imaginary components represent the estimated impedance obtained from the conventional distance relay model under different network topologies.

Slight variations in the impedance observed at different fault locations are mainly due to changes in the magnitude of the infeed current contribution to the faulted section of the line. The results indicate a slight decrease in the estimated impedance because of current infeed contributions from the integrated renewable energy sources.

Table 3
Estimated impedance under short-circuit fault scenarios

km	Estimated Impedance with Renewable (Ω)			Estimated Impedance with Renewable (Ω)			% Impedance Difference (Ω)
	R	X	Z∠θ	R	X	Z∠θ	
20	1.71	6.43	6.66∠84.56	1.94	6.37	7.67∠84.50	1.012
40	3.16	12.90	13.31∠84.54	3.93	12.70	14.31∠84.52	1.001
60	3.617	19.3	19.94∠84.64	5.705	19.0	20.94∠84.53	1.590
80	5.03	26.1	26.57∠84.60	7.81	25.3	27.57∠84.52	1.000
100	3.393	32.6	33.20∠84.72	8.83	31.8	34.20∠84.55	1.000
120	4.66	39.5	39.83∠84.70	10.66	38.3	39.99∠84.50	0.160
140	3.2	46.3	48.40∠84.70	11.22	45.0	48.66∠84.58	0.400
160	5.63	53.1	53.15∠84.81	11.84	51.8	53.20∠84.60	0.094
180	3.14	59.7	59.89∠81.88	12.56	58.7	60.01∠84.61	0.200
200	8.39	66.0	66.56∠84.95	12.41	65.9	67.08∠84.60	0.778

This reduction in impedance below the preset threshold value indicates the occurrence of short-circuit faults during power swing and fault conditions. The infeed current, therefore, compromises the preset impedance threshold of the distance relay by producing a lower estimated value, which leads to a faster movement of the impedance trajectory into the relay operating zone and may initiate an unintended trip command.

Estimated Impedance Under Power Swing Conditions

The results presented in Table 4 demonstrate the impact of renewable energy integration on the magnitude of power swings (PS), primarily influenced by the infeed current

Table 4
Estimated impedance under power swing scenarios

km	Estimated Impedance with Renewable (Ω)			Estimated Impedance with Renewable (Ω)			% Impedance Difference (Ω)
	R	X	Z∠θ	R	X	Z∠θ	
20	0.125	6.54	6.55∠87.95	0.13	6.54	7.55∠87.95	1.000
40	0.15	13.11	13.11∠87.95	0.15	13.11	14.19∠87.95	1.080
60	0.214	19.68	19.68∠87.95	0.21	19.68	19.99∠87.95	0.030
80	0.32	26.28	28.28∠87.95	0.32	26.28	29.23∠87.95	0.950
100	0.519	32.91	32.91∠87.95	0.52	32.91	32.99∠87.95	0.080
120	0.89	39.58	39.58∠87.95	0.88	39.58	39.88∠87.95	0.300
140	1.27	46.29	46.31∠87.95	1.27	46.29	46.71∠87.95	0.400
160	1.87	53.07	53.10∠87.95	2.9	53.11	53.19∠87.95	0.169
180	2.43	59.90	59.95∠87.92	4.3	60.13	60.28∠87.95	0.549
200	3.26	66.81	66.81∠87.95	6.03	67.23	67.50∠87.95	0.908

contributions from the interconnected sources. These results indicate that renewable energy integration has a noticeable effect on the estimated impedance observed by the distance relay during power swing events, particularly considering the intermittent nature of renewable energy sources.

A slight variation in the impedance estimated by the distance relay is observed between the two network topologies. This variation is mainly attributed to the additional infeed current contributions from the integrated renewable energy generating sources.

Power swing events often exhibit characteristics like those observed during symmetrical short-circuit faults. However, the key difference lies in the rate of change of the impedance locus. During power swing conditions, the impedance locus changes more gradually, resulting in a slower movement of the impedance trajectory toward the relay trip operating zone. As the estimated impedance gradually encroaches into the relay's trip region due to its reduced magnitude, the relay may issue an instantaneous trip command to the associated circuit breakers, potentially leading to unintended operations.

Intelligent Machine Learning-PSB Classifier Model Results

The development of the Power Swing Blocking (PSB) predictive classifier model is formulated as a binary classification problem aimed at discriminating between stable power swing (PS) conditions and symmetrical three-phase short-circuit faults occurring under similar operating conditions. The intelligent ML-PSB function classifier model for the distance relay was developed using balanced simulation scenario event records.

Each event scenario, representing either three-phase symmetrical faults or stable power swings, consisted of 3,078 historical event instances. Sixteen selected system operational features extracted from the simulated dataset were used to develop the intelligent ML-PSB predictive model. Several supervised machine learning algorithms were evaluated using the WEKA data mining environment to determine the most suitable classification model.

Intelligent ML-PSB Model Algorithm Selection

The best-performing classification algorithms were selected from different machine learning categories based on statistical evaluation indices. These indices included the true positive rate (TP), true negative rate (TN), false positive rate (FP), and false negative rate (FN). Additional performance metrics such as precision, recall, F-measure, receiver operating characteristic (ROC), and computational time were also considered.

Table 5 contains a summary of the algorithms illustrating superior performance benchmarked against the baseline model. This fulfils the chosen statistical performance criteria.

Table 5
Deployed ML algorithms for the ML-PSB function model

Categories	**Algorithm names**	**Classification (%)**		**Precision**	**Recall**	**ROC Curve**	**Time (s)**
		Correct	**Incorrect**				
Baseline	ZeroR*	49,862	50,138	0,498	0,499	0,498	0
	PART	100	0	1	1	1	0,05
	JRip	100	0	1	1	1	0,11
	DecisionTable	100	0	1	1	1	0,39
Trees	DecisionStump	100	0	1	1	1	0,03
	Hoeffding	100	0	1	1	1	0,09
	J48*	100	0	1	1	1	0
	RandomForest	100	0	1	1	1	0,34
	RandomTree*	100	0	1	1	1	0
	REPTree	100	0	1	1	1	0,03
Meta Ensemble	AdaBoostM1	100	0	1	1	1	0,03
	Bagging	100	0	1	1	1	0,12
	FilteredClassifier	100	0	1	1	1	0,06
	LogitBoost	100	0	1	1	1	0,2
	MultiClassClassifier	100	0	1	1	1	0,09
	RandomCommittee	100	0	1	1	1	0,03
	RandomSubSpace	100	0	1	1	1	0,05
	Vote	49,862	50,138	0,5	0,5	-0,5	0
Lazy	IBK	100	0	1	1	1	0
	LWL*	100	0	1	1	1	0
Functions	Logistic*	100	0	1	1	1	0,02
	MultilayerPerceptron	100	0	1	1	1	10,86
	SGDText	50	50	-	0,5	0,5	0,2
	SimpleLogistic	100	0	1	1	1	0,63
	SMO	100	0	1	1	1	0,05
Bayes	BayesNet	100	0	1	1	1	0,08
	NaiveBayes	99,346	0,6536	0,994	0,993	0,991	0,02
	NaiveBayesUpdateable*	99,3464	0,6536	0,994	0,993	0,991	0

ML-PSB Classifier Model Performance Evaluation

Optimal model selection criteria were employed to further examine the chosen algorithms as highlighted in Table 6. This was done to recognise the most suitable classifier model which can fulfil the operational challenges of the distance relay in the WEKA experimental framework. Special attention was paid to minimising the computational time while still trying to retain the accuracy of the classification.

This requirement is critical because the operating time of conventional distance relay trip decisions is approximately one cycle (20 ms). The novelty of the present study lies in improving this response time by selecting an algorithm capable of near-instantaneous response, achieving an operating time of approximately 10 ms.

Four evaluation criteria were used to determine the most suitable ML-PSB model: F-measure, classification accuracy, recall, and computational response time. Statistical comparisons were performed using a 0.05 significance level with t-test indicators.

The results show that the RandomTree algorithm achieved superior performance, demonstrating approximately 95% statistical significance across the evaluated performance metrics compared with the other five candidate algorithms. As illustrated in Figure 11, RandomTree achieved the highest performance in terms of F-measure, precision, recall, and computational efficiency.

The F-measure, calculated from the harmonic mean of precision and recall, further confirmed the RandomTree algorithm as the most suitable ML-PSB classifier model for detecting and discriminating stable power swings from three-phase symmetrical faults.

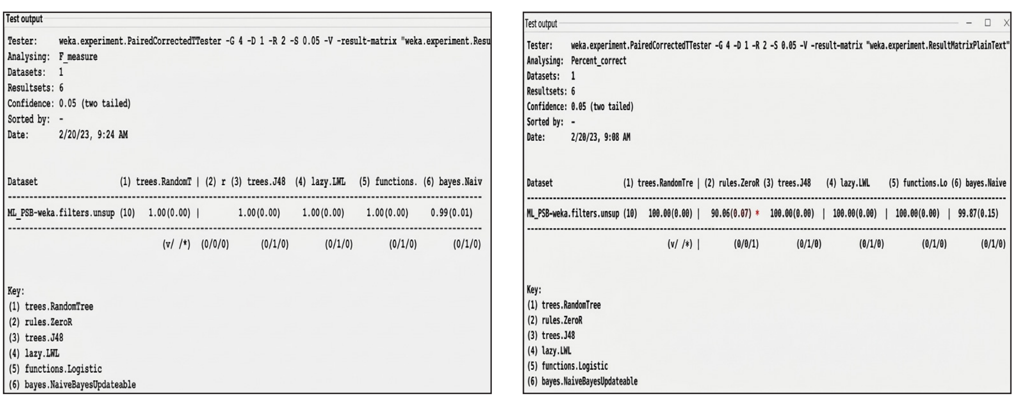

(a) (b)

Figure 11. Statistical algorithm model comparison for the PSB function based on (a) F-measure, (b) accuracy, (c) recall, and (d) response time

RandomTree-PSB Classifier Model Performance

The performance evaluation results of the developed RandomTree-PSB model using an independent test dataset are presented in Figure 12. This dataset was not used during the model training stage, allowing the model's generalisation capability to be properly assessed.

The performance indicators were derived from the confusion matrix results, where the diagonal elements represent correctly classified event scenarios, while the off-diagonal elements represent misclassified events.

=== Stratified cross-validation ===
=== Summary ===

Correctly Classified Instances	6156	100	%
Incorrectly Classified Instances	0	0	%
Kappa statistic	1		
Mean absolute error	0		
Root mean squared error	0		
Relative absolute error	0	%	
Root relative squared error	0	%	
Total Number of Instances	6156		

=== Detailed Accuracy By Class ===

	TP Rate	FP Rate	Precision	Recall	F-Measure	MCC	ROC Area	PRC Area	Class
	1.000	0.000	1.000	1.000	1.000	1.000	1.000	1.000	block-trip
	1.000	0.000	1.000	1.000	1.000	1.000	1.000	1.000	trip
Weighted Avg.	1.000	0.000	1.000	1.000	1.000	1.000	1.000	1.000	

=== Confusion Matrix ===

<-- classified as

Actual \ Predicted	a (block-trip)	b (trip)
a (block-trip)	612	0
b (trip)	0	5544

Class Mapping
a = block-trip
b = trip

Figure 12. RandomTree-PSB model test performance results

The intelligent PSB model successfully classified all 6,156 test instances without misclassification, demonstrating a classification accuracy of 100%. A total of 612 event scenarios were correctly classified as stable power swings (true positives), resulting in a trip-blocking command issued by the ML-PSB function. Among all the classifications that were recorded, there were no false positive classifications.

In the same vein, the model correctly classified 5,544 cases as fault events, which permit the ML-PSB scheme to release a trip signal to the relevant circuit breakers without hesitation to protect the system. The high number of correctly classified scenarios shows that the RandomTree-PSB model was able to efficiently distinguish between symmetrical short-circuit faults and stable power swing scenarios.

The results went further to show that the proposed model ensured good classification accuracy across different operating scenarios, which indicates that it learned the underlying characteristics of both events rather than ordinarily memorizing the training data. Adding to that, the intelligent PSB scheme acted considerably faster than the traditional PSB function and the relay operating time was reduced from about 20 ms to approximately 10 ms. This can contribute to faster fault isolation and enhanced protection performance. As shown in Figure 13, the decision-making process of the RandomTree-PSB model is represented by the generated decision tree.

The pseudocode for the RandomTree algorithm is presented below:

1. **Input:** Test dataset
    a. Apply each randomly generated decision tree to the test dataset and record its predicted output.
    b. Count the number of votes received for every class label.
    c. Select the class with the highest number of votes as the final prediction.
2. **Output:** Final predicted class label.

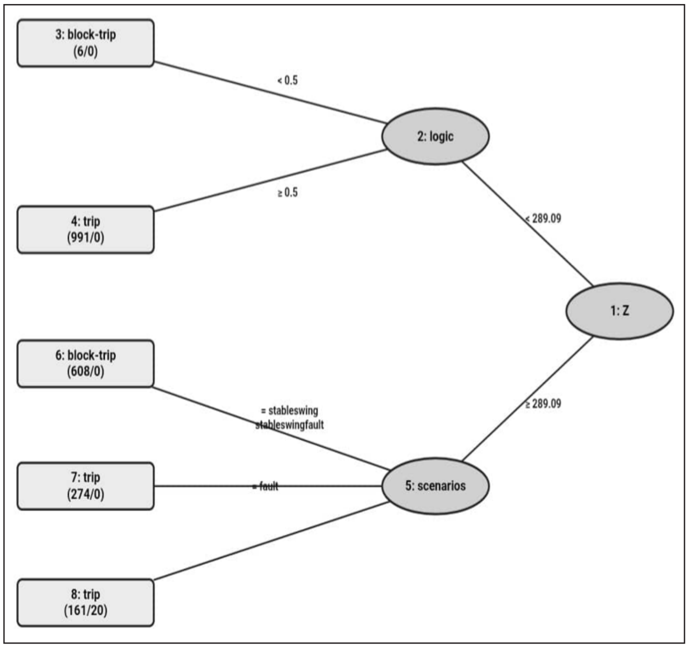

Figure 13. RandomTree-PSB decision tree

Intelligent Machine Learning–OST Classifier Model Results

The second intelligent protection function developed in this study is the Machine Learning-based Out-of-Step Tripping (ML-OST) classifier. Like the PSB model, the ML-OST function is formulated as a binary classification model designed to distinguish between stable and unstable power swing conditions during power system disturbances.

The dataset used for this model consisted of 612 stable power swing records and 608 unstable swing records obtained from simulated system disturbances. These datasets were used to train and evaluate the ML-OST classifier for accurate detection and classification of swing stability conditions.

Intelligent ML-OST Algorithm Selection

Multiple machine learning algorithms were evaluated for the ML-OST classifier development using the same performance evaluation metrics applied to the ML-PSB model. These metrics included classification accuracy, precision, recall, ROC performance, and computational time.

Algorithms that demonstrated accuracy above the baseline model and lower computational time were selected for further evaluation. The machine learning algorithms are depicted in Table 6.

In developing the intelligent OST classifier, the sensitivity requirements of the traditional OST function were taken into consideration to make sure that stable and unstable

Table 6
Deployed ML algorithms for the ML-OST function model

Categories	Algorithm names	Classification (%)		Precision	Recall	ROC Curve	Time (s)
		Correct (%)	Incorrect (%)				
Baseline	ZeroR*	49,862	50,138	0,498	0,499	0,498	0
	PART	100	0	1	1	1	0,05
	JRip	100	0	1	1	1	0,11
	DecisionTable	100	0	1	1	1	0,39
Trees	DecisionStump	100	0	1	1	1	0,03
	Hoeffding	100	0	1	1	1	0,09
	J48*	100	0	1	1	1	0
	RandomForest	100	0	1	1	1	0,34
	RandomTree*	100	0	1	1	1	0
	REPTree	100	0	1	1	1	0,03
Meta Ensemble	AdaBoostM1	100	0	1	1	1	0,03
	Bagging	100	0	1	1	1	0,12
	FilteredClassifier	100	0	1	1	1	0,06
	LogitBoost	100	0	1	1	1	0,2
	MultiClassClassifier	100	0	1	1	1	0,09
	RandomCommittee	100	0	1	1	1	0,03
	RandomSubSpace	100	0	1	1	1	0,05
	Vote	49,862	50,138	0,5	0,5	-0,5	0
Lazy	IBK	100	0	1	1	1	0
	LWL*	100	0	1	1	1	0
	Logistic*	100	0	1	1	1	0,02
Functions	MultilayerPerceptron	100	0	1	1	1	10,86
	SGDText	50	50	-	0,5	0,5	0,2
	SimpleLogistic	100	0	1	1	1	0,63
	SMO	100	0	1	1	1	0,05
Bayes	BayesNet	100	0	1	1	1	0,08
	NaiveBayes	99,346	0,6536	0,994	0,993	0,991	0,02
	NaiveBayesUpdateable*	99,3464	0,6536	0,994	0,993	0,991	0

power swing conditions are identified correctly. Improving the performance of the OST protection operation is important because an incorrect relay operation during a power swing can initiate additional relay actions elsewhere in the network, which increases the chances of widespread system perturbation and, in severe cases, leads to a system blackout.

ML-OST Model Performance Evaluation

The selected algorithms were subsequently evaluated using a range of machine learning performance metrics. These metrics included classification accuracy, precision, recall, F-measure, and computational response time. The objective was to assess both the classification capability and the practical suitability of each algorithm for protection applications.

The comparative results obtained are presented in Figure 14. Among the evaluated algorithms, the RandomTree model achieved the most favourable overall performance, thereby outperforming the other shortlisted techniques across the selected evaluation criteria.

RandomTree-OST Classifier Model Performance

Among the five machine learning algorithms evaluated, the RandomTree model gave the best overall results for the proposed intelligent OST operation. The model achieved a classification accuracy of 99.7%, which successfully classified 1,218 power swing events

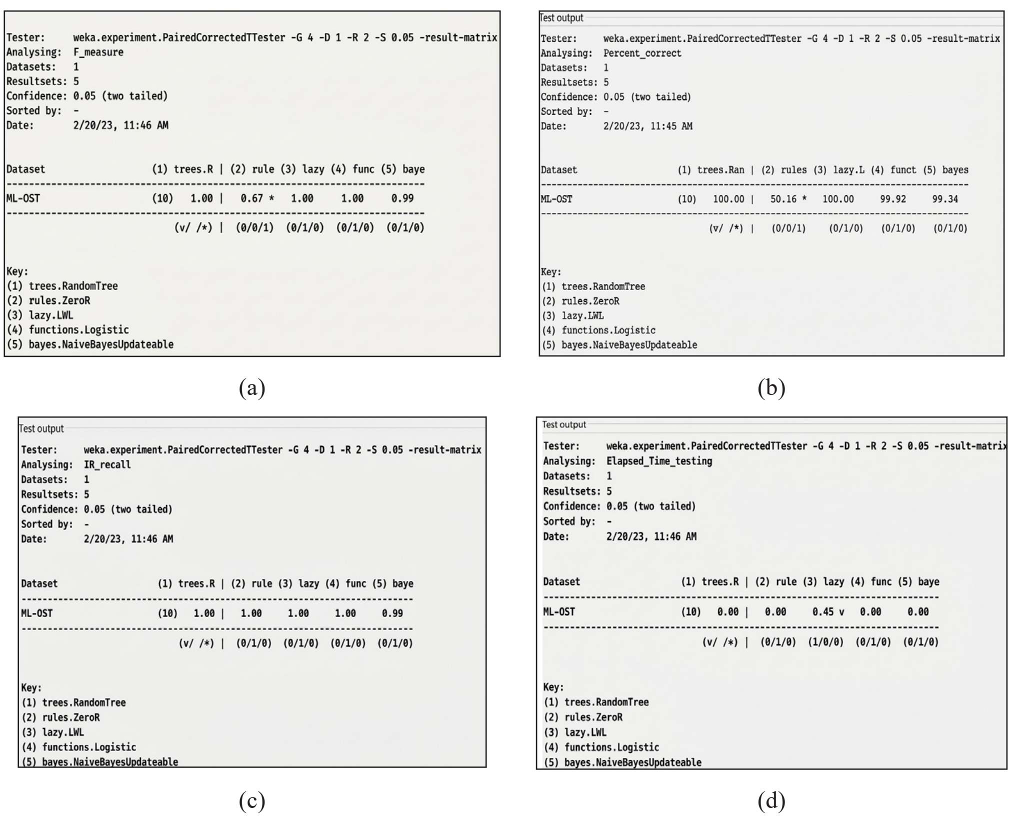

Figure 14. Statistical comparison of the evaluated algorithms for the OST operation based on (a) F-measure, (b) classification accuracy, (c) recall, and (d) response time

into stable and unstable swing categories. From the simulation, only two events were misassigned to the wrong class during testing.

The classification results obtained are summarised in the confusion matrix shown in Figure 15. The values along the main diagonal depict events that were classified properly, while the off-diagonal entries correspond to misclassified cases.

Out of the evaluated events, 612 stable power swing scenarios were identified properly, and this resulted in the OST operation blocking an unwanted trip signal. Only two stable power swing events were assigned to the improper category.

In the case of unwanted scenarios, all 608 events were identified properly by the model. During these conditions, the OST operation gave a trip command to the responsible circuit breakers to open the affected section of the network and maintain system security. Here, no unstable power swing scenarios were misclassified as stable swings during the evaluation process.

The decision tree structure generated by the RandomTree-OST classifier is shown in Figure 16. The model primarily utilises frequency and magnitude-related system features to discriminate between stable and unstable power swing conditions.

Voltage and current signal features extracted from the simulated datasets contribute varying levels of decision information across different stages of the classification process. The developed RandomTree-OST model demonstrated strong adaptability to different network configurations and varying infeed current contributions resulting from renewable energy integration.

The results confirm that the intelligent OST model significantly improves the response time and classification performance compared with conventional OST protection schemes. This improvement reduces the likelihood of cascading protection failures that could otherwise lead to large-scale grid disturbances.

```
=== Stratified cross-validation ===
=== Summary ===

Correctly Classified Instances        1218               99.8361 %
Incorrectly Classified Instances         2                0.1639 %
Kappa statistic                          0.9967
Mean absolute error                      0.0016
Root mean squared error                  0.0405
Relative absolute error                  0.3279 %
Root relative squared error              8.0978 %
Total Number of Instances             1220

=== Detailed Accuracy By Class ===

                 TP Rate  FP Rate  Precision  Recall   F-Measure  MCC      ROC Area  PRC Area  Class
                 0.997    0.000    1.000      0.997    0.998      0.997    0.998     0.998     block-trip
                 1.000    0.003    0.997      1.000    0.998      0.997    0.998     0.997     trip
Weighted Avg.    0.998    0.002    0.998      0.998    0.998      0.997    0.998     0.998

=== Confusion Matrix ===

   a   b   <-- classified as
 610   2 |   a = block-trip
   0 608 |   b = trip
```

Figure 15. RandomTree-OST model performance results

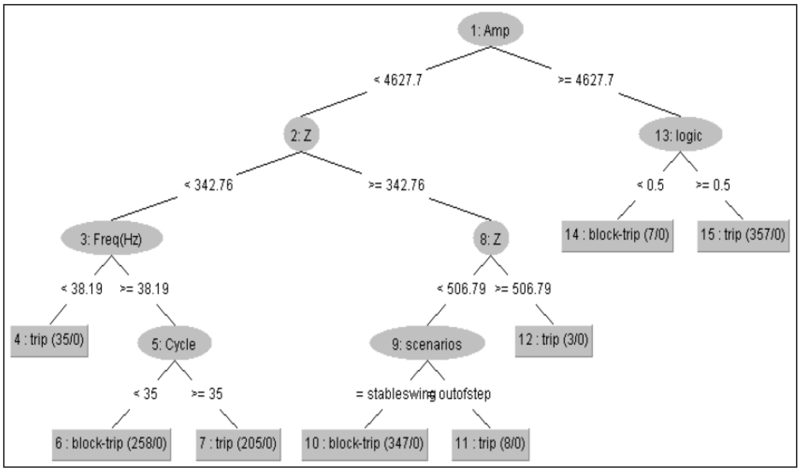

Figure 16. RandomTree ML-OST decision tree

CONCLUSION

The following conclusions are drawn from the results presented in this study:

The first objective of the study demonstrated that current infeed contributions from integrated renewable energy sources (wind farms) significantly influence the magnitude of power swings within the power system. These contributions affect the impedance estimation of the distance relay and may lead to relay maloperation during stable power swing conditions.

To address this limitation, an intelligent RandomTree-PSB classifier model was developed to enhance the performance of the conventional Power Swing Blocking function. The proposed model achieved 100% classification accuracy with a response time of approximately 10 ms, representing a significant improvement over the conventional relay response time of approximately 20 ms.

The intelligent RandomTree-OST classifier model effectively discriminates between stable and unstable power swing conditions. The model achieved a classification accuracy of 99.7% with an operating time of approximately 10 ms, demonstrating improved performance compared with conventional OST relay functions.

Overall, the proposed intelligent PSB and OST models significantly improve the reliability, speed, and accuracy of distance relay protection in renewable energy-integrated power systems.

ACKNOWLEDGEMENT

We, the authors, would like to thank Prof. Ir. Dr Mohammad Lutfi Othman for his guidance, support and constructive feedback throughout the course of this research. His advice and encouragement were greatly appreciated and contributed significantly to the completion of this work. We also wish to acknowledge Assoc. Prof. Dr Hashim Hizam and Prof. Ir. Dr Mohd Zainal Abdin Ab Kadir for their valuable comments, technical input and suggestions during the study. Their contributions helped strengthen various aspects of the research. The authors further extend their appreciation to the academic and technical staff of the Department of Electrical and Electronic Engineering, Faculty of Engineering, Universiti Putra Malaysia, and to members of the Advanced Lightning, Power and Energy Research (ALPER) Group for their assistance, support and the positive research environment provided throughout this work.

REFERENCES

Abdi-Khorsand, M., & Vittal, V. (2016). Modelling protection systems in time-domain simulations: A new method to detect mis-operating relays for unstable power swings. *IEEE Transactions on Power Systems, 32*(4), 2790-2798. https://doi.org/10.1109/TPWRS.2016.2628726

Adak, S. (2024). Power factor analysis of grid-connected solar inverter under different irradiance levels throughout the day. *Energies, 17*(15), Article 3632. https://doi.org/10.3390/en17153632

Ali, N. H., Ali, B. M., Basri, O., Husin, N. L., & Abdel-Latif, K. M. (2016). Protection of smart substation based on WLAN complies with IEC 61850 using travelling wave analysis. *Electric Power Systems Research, 140*, 20-26. https://doi.org/10.1016/j.epsr.2016.07.004

Arumuga, M., & Reddy, M. J. B. (2022). Distance protection methodology for detection of faulted phase and fault along with power swing using apparent impedance. *IEEE Access, 10*, 43583-43597. https://doi.org/10.1109/ACCESS.2022.3168563

Audu, N. A., Alphaeus, O., & Adamu, T. (2018). Effect of inertia constant on generator frequency and rotor angle. *Engineering and Applied Science, 3*(1), Article 6. https://doi.org/10.11648/j.eas.20180301.12

Chaitanya, M. N., & Rao, G. S. K. (2019). A novel scheme for supervising third zone distance relay operation during power swings. In *2019 International Conference on Computing, Power and Communication Technologies (GUCON)* (pp. 41-46). IEEE.

Chothani, N. G., Bhalja, B. R., & Parikh, U. B. (2014). New support vector machine-based digital relaying scheme for discrimination between power swing and fault. *IET Generation, Transmission & Distribution, 8*(1), 17-25. https://doi.org/10.1049/iet-gtd.2013.0020

Dreidy, M., Mokhlis, H., & Mekhilef, S. (2017). Inertia response and frequency control techniques for renewable energy sources: A review. *Renewable and Sustainable Energy Reviews, 69*, 144-155. https://doi.org/10.1016/j.rser.2016.11.170

Fang, Y., Jia, K., Yang, Z., Li, Y., & Bi, T. (2018). Impact of inverter-interfaced renewable energy generators on distance protection and an improved scheme. *IEEE Transactions on Industrial Electronics, 66*(9), 7078-7088. https://doi.org/10.1109/TIE.2018.2873521

Fischer, N., Benmouyal, G., Hou, D., Tziouvaras, D., Byrne-Finley, J., & Smyth, B. (2012). Tutorial on power swing blocking and out-of-step tripping. In *Proceedings of the 39th Annual Western Protective Relay Conference*.

Gautam, D., Vittal, V., & Harbour, T. (2009). Impact of increased penetration of DFIG-based wind turbine generators on transient and small signal stability of power systems. *IEEE Transactions on Power Systems, 24*(3), 1426-1434. https://doi.org/10.1109/TPWRS.2009.2021234

Gonzalez-Longatt, F., Adiyabazar, C., & Martinez, E. V. (2021). Setting and testing of the out-of-step protection at Mongolian transmission system. *Energies, 14*(23), Article 8170. https://doi.org/10.3390/en14238170

Haddadi, A., Farantatos, E., Kocar, I., & Karaagac, U. (2021). Impact of inverter-based resources on system protection. *Energies, 14*(4), Article 1050. https://doi.org/10.3390/en14041050

Haddadi, A., Kocar, I., Karaagac, U., Gras, H., & Farantatos, E. (2019). Impact of wind generation on power swing protection. *IEEE Transactions on Power Delivery, 34*(3), 1118-1128. https://doi.org/10.1109/TPWRD.2019.2896135

Jafari, R., Moaddabi, N., Eskandari-Nasab, M., Gharehpetian, G., & Naderi, M. (2014). A novel power swing detection scheme independent of the rate of change of power system parameters. *IEEE Transactions on Power Delivery, 29*(3), 1192-1202. https://doi.org/10.1109/TPWRD.2013.2297625

Kang, D., & Gokaraju, R. (2016). A new method for blocking third-zone distance relays during stable power swings. *IEEE Transactions on Power Delivery, 31*(4), 1836-1843. https://doi.org/10.1109/TPWRD.2016.2520394

Khan, A., Hizam, H., Abdul Wahab, N. I., & Othman, M. L. (2020). Solution of optimal power flow using non-dominated sorting multi-objective based hybrid firefly and particle swarm optimisation algorithm. *Energies, 13*(16), Article 4265. https://doi.org/10.3390/en13164265

Kumar, V., Pandey, A., & Sinha, S. (2016). Grid integration and power quality issues of wind and solar energy systems: A review. In *ICETEESES 2016* (pp. 71-80). IEEE. https://doi.org/10.1109/ICETEESES.2016.7581355

Mooney, P. J., & Fischer, N. (2006). Application guidelines for power swing detection on transmission systems. In *Power Systems Conference* (pp. 159-168). IEEE. https://doi.org/10.1109/PSAMP.2006.285385

Nasab, M. R., & Yaghobi, H. (2020). A real-time out-of-step protection strategy based on instantaneous active power deviation. *IEEE Transactions on Power Delivery, 36*(6), 3590-3600. https://doi.org/10.1109/TPWRD.2020.3045276

Niknezhad, M., & Sadeh, J. (2022). Analysis of wind farm penetration on power swing detection in distance relays. *IET Renewable Power Generation, 16*(2), 375-388. https://doi.org/10.1049/rpg2.12333

Nwaigwe, K., Mutabilwa, P., & Dintwa, E. (2019). An overview of solar power integration into electricity grids. *Materials Science for Energy Technologies, 2*(3), 629-633. https://doi.org/10.1016/j.mset.2019.07.002

Okeke, C. O., Lutfi, O. M., Hashim, H., Kadir, M. Z. A., Wahab, N. I. A., Emmanuel, O., Nwagbara, S., & Chimeleze, C. (2023). Renewable energy impact on distance relay power swing blocking and fault discrimination: A review. *Pertanika Journal of Science & Technology, 31*(6), 2887-2913. https://doi.org/10.47836/pjst.31.6.14

Paudyal, S., Ramakrishna, G., & Sachdev, M. S. (2010). Application of equal area criterion conditions in the time domain for out-of-step protection. *IEEE Transactions on Power Delivery, 25*(2), 600-609. https://doi.org/10.1109/TPWRD.2009.2032326

Sabo, A., Abdul Wahab, N. I., Othman, M. L., Jaffar, M. Z. A. M., Beiranvand, H., & Akçayol, M. (2020). Application of neuro-fuzzy controller to replace SMIB and interconnected multi-machine power system stabilisers. *Sustainability, 12*(22), Article 9591. https://doi.org/10.3390/su12229591

Shair, J., Li, H., Hu, J., & Xie, X. (2021). Power system stability issues, classifications and research prospects in the context of high penetration of renewables and power electronics. *Renewable and Sustainable Energy Reviews, 145*, Article 111111. https://doi.org/10.1016/j.rser.2021.111111

Telukunta, V., Pradhan, J., Agrawal, A., Singh, M., & Srivani, S. G. (2017). Protection challenges under bulk penetration of renewable energy resources in power systems: A review. *CSEE Journal of Power and Energy Systems, 3*(4), 365-379. https://doi.org/10.17775/CSEEJPES.2017.00030

Veerasamy, V., Abdul Wahab, N. I., Ramachandran, R., Othman, M. L., Hizam, H., Devendran, V. S., Irudayaraj, A. X. R., & Vinayagam, A. (2021). Recurrent network-based power flow solution for voltage stability assessment and improvement with distributed energy sources. *Applied Energy, 302*, Article 117524. https://doi.org/10.1016/j.apenergy.2021.117524

Verzosa, Q. (2013). Realistic testing of power swing blocking and out-of-step tripping functions. In *Proceedings of the 66th Annual Conference for Protective Relay Engineers* (pp. 420-449). IEEE. https://doi.org/10.1109/CPRE.2013.6822056

Wei, Q., Han, X., Guo, W., Yang, M., & He, N. (2014). The principle of absolute rotor angle control and its effect on suppressing inter-area low-frequency oscillations. *International Journal of Electrical Power & Energy Systems, 63*, 1039-1046. https://doi.org/10.1016/j.ijepes.2014.07.006

Yellajosula, J. R. A. K., Wei, Y., Grebla, M., Paudyal, S., & Mork, B. A. (2019). Online detection of power swing using approximate stability boundaries. *IEEE Transactions on Power Delivery, 35*(3), 1220-1229. https://doi.org/10.1109/TPWRD.2019.2941522

Zhang, Z., Jacques, A., & Voloh, I. (2016). Challenges in application of distance relays under power swing conditions. In *Proceedings of the 69th Annual Conference for Protective Relay Engineers (CPRE)*. IEEE. https://doi.org/10.1109/CPRE.2016.7914882